ORIGINAL PAPER

Single-crystal elastic properties of alunite, $KAl_3(SO_4)_2(OH)_6$

**J. Majzlan · S. Speziale · T. S. Duffy ·
P. C. Burns**

Abstract The single-crystal elastic constants of natural alunite (ideally $KAl_3(SO_4)_2(OH)_6$) were determined by Brillouin spectroscopy. Chemical analysis by electron microprobe gave a formula $KAl_3(SO_4)_2$ $(OH)_6$. Single crystal X-ray diffraction refinement with $R_1 = 0.0299$ for the unique observed reflections $(|F_o| > 4\sigma_F)$ and $wR_2 = 0.0698$ for all data gave $a = 6.9741(3)$ Å, $c = 17.190(2)$ Å, fractional positions and thermal factors for all atoms. The elastic constants (in GPa), obtained by fitting the spectroscopic data, are $C_{11} = 181.9 \pm 0.3$, $C_{33} = 66.8 \pm 0.8$, $C_{44} = 42.8 \pm 0.2$, $C_{12} = 48.2 \pm 0.5$, $C_{13} = 27.1 \pm 1.0$, $C_{14} = 5.4 \pm 0.5$, and $C_{66} = \frac{1}{2}(C_{11} - C_{12}) = 66.9 \pm 0.3$ GPa. The VRH averages of bulk and shear modulus are 63 and 49 GPa, respectively. The aggregate Poisson ratio is 0.19. The high value of the ratio $C_{11}/C_{33} = 2.7$ and of the ratio $C_{66}/C_{44} = 1.6$ are characteristic of an anisotropic structure with very weak interlayer interactions along the c-axis. The basal plane (001) is characterized by 0.1% longitudinal acoustic anisotropy and 0.9–1.1% shear acoustic anisotropy, which gives alunite a characteristic pseudo-hexagonal elastic behavior, and is related to the pseudo-hexagonal arrangement of the $Al(O,OH)_6$ octahedra in the basal layer. The elastic Debye temperature of alunite is 654 K. The large discrepancy between the elastic and heat capacity Debye temperature is also a consequence of the layered structure.

Introduction

Hydrated iron and aluminum sulfates attract attention because they are associated with acid mine drainage, a widely recognized environmental problem (Jambor et al. 2000). The geochemical implications of acid mine drainage generation and its environmental effects have been addressed in numerous field and laboratory studies (e.g., Blowes et al. 1998; Cravotta et al. 1999; Hudson-Edwards et al. 1999). Among the latter, computer simulations of solids or aqueous solutions are used to support the experimental results or provide information not available in experimental studies (e.g., Becker and Gasharova 2001). These calculations have the capability of providing reliable data about processes on a molecular scale. To meet this goal, either sophisticated (i.e., first principles) methods have to be employed, with the trade-off of only small systems being simulated, or good quality empirical interatomic potentials must be available. Derivation of reliable empirical potentials requires at least the knowledge of the crystal structure (lattice parameters, atomic positions), but can be much more reliable if dielectric, elastic, or thermodynamic quantities are also known.

J. Majzlan (✉)
Institute of Mineralogy and Geochemistry,
Albert-Ludwig-University of Freiburg,
Alberstraße 23b, 79104 Freiburg, Germany
e-mail: juraj.majzlan@minpet.uni-freiburg.de

S. Speziale · T. S. Duffy
Department of Geosciences, Princeton University,
Princeton, NJ 08544, USA

P. C. Burns
Department of Civil Engineering and Geological Science,
University of Notre Dame, Notre Dame, IN 46556, USA

There is also increasing interest in sulfates as important components of planetary surfaces. Hydrated sulfates have been identified on the surface of Jupiter's satellite Europa and these may have been produced from interactions involving a subsurface ocean (McCord et al. 2001; Zolotov and Shock 2001). Sulfates are also present on the surface of Mars (Blaney and McCord 1995; Klingelhofer et al. 2004). Characterization of the elastic properties of hydrous sulfates is an important step in constraining the overall thermodynamics of such phases, especially as the elastic tensor allows reliable determination of the bulk modulus.

In this paper, we report the elastic constants of alunite measured by Brillouin spectroscopy. Alunite is an excellent candidate for intermolecular potential development and testing because its structure is known well, including the hydrogen positions (Schukow et al. 1999). Moreover, alunite is a common sulfate mineral found in high-sulfidation hydrothermal systems and sedimentary environments (Stoffregen and Alpers 1992), and is closely related to the mineral jarosite reported to occur on the surface of Mars (Klingelhofer et al. 2004). The data presented in this paper can therefore serve for the derivation of new or improvement of existing potentials (force fields) and thus aid in modeling of natural systems that contain alunite and other sulfate minerals.

Our original intention was also to measure elastic constants of jarosite (Fe^{3+} analog of alunite) and other selected ferric iron sulfates. However, we found that compounds whose major component is Fe^{3+} absorb the incident laser beam so strongly that Brillouin scattering measurements were not feasible with our system.

Experimental procedures

The samples used in this study were hand-picked from a druse of tabular alunite crystals from Chinkuahshih mine, Taiwan. Single crystal X-ray diffraction (XRD) data were collected for a suitable single crystal using a Bruker three-circle diffractometer equipped with an APEX CCD detector and Mo Kα radiation. A sphere of diffraction data to 69 °2Θ was collected at room temperature using a crystal-to-detector distance of 4.67 cm, frame widths of 0.3° in ω, and 10 s spent counting per frame. Intensity data were reduced and corrected for Lorentz, polarization, and background effects using the Bruker program SAINT.

Scattering curves for neutral atoms and anomalous-dispersion corrections were taken from Ibers and Hamilton (1974). The Bruker SHELXTL Version 5 system of programs was used for the solution and refinement of the crystal structure in space group $R\bar{3}m$. The final refinement included positional parameters of all atoms, anisotropic displacement parameters for non-H atoms, and a weighting scheme of the structure factors.

A powder XRD pattern was collected with a Scintag PAD V diffractometer, equipped with a Cu radiation source, diffracted-beam monochromator, and a scintillation detector. The pattern was collected in a flat-plate geometry. Lattice parameters were derived by Rietveld refinement using GSAS (Larson and von Dreele 1994). The chemical composition of the sample was measured by a CAMECA SX100 electron microprobe with standards orthoclase (K), hematite (Fe), barite (S), albite (Na), corundum (Al), periclase (Mg), rhodonite (Mn), and wollastonite (Ca), and conditions 15 nA, 15 kV, and beam size of 15 μm. Back-scattered electron images (BSEI) were acquired with the same instrument.

The Brillouin scattering experiments were performed on two plane-parallel platelets with orientation (001) and (–0.86, –0.72, 1), cut from the same crystal. The two platelets, 2–3 mm wide, were ground to 200 μm thickness and their faces were polished to submicron finish. The parallelism of the platelets' faces was controlled within 0.001° (see Jiang et al. 2004). The platelets were mounted on a vertical goniometer stage and Brillouin scattering was measured along 36 different directions selected along the platelets by incremental 5° rotations of the goniometer. Every spectrum was collected for 5 min.

Brillouin experiments were performed in 80° forward symmetric scattering geometry. The 532 nm line of a Nd:YVO$_4$ laser operated at a power of 1.6 W and filtered to 160 mW was used as an excitation source. Inelastically scattered photons were analyzed by a six-pass Sandercock tandem Fabry-Perot interferometer (Lindsay et al. 1981) and recorded by a solid-state detector. Further details about the arrangement of the optical elements and the accuracy and precision are given by Speziale and Duffy (2002). Temperature of the measurement was 295 ± 1 K.

Results

The results of the single-crystal XRD analysis are summarized in Table 1. The crystal structure of our sample corresponds to that determined by Hendricks (1937); layers of corner-shared Al(O,OH)$_6$ octahedra are decorated by sulfate tetrahedra (Fig. 1). The interlayer portions of the structure are occupied by monovalent cations, mostly K^+. The sites of monovalent

Table 1 Atomic positions, displacement factors ($\text{Å}^2 \times 10^3$), unit-cell parameters, and data statistics for the refinement of the XRD data for alunite

Atom	x	y	z	Occupancy	Wyckoff position
S	0	0	0.30380(4)	1	6c
Al	0	1/2	1/2	0.989(3)	9d
O1	0	0	0.3882(1)	1	6c
O2	0.2182(1)	−0.2182(2)	−0.0591(1)	1	18h
O3	0.1258(1)	−0.1258(1)	0.1400(1)	1	18h
K	0	0	0	0.805(9)	3a
Na	0	0	0	0.132(2)	
O4	0	0	0	0.063(11)	
H	0.178(3)	−0.178(3)	0.118(2)	1	18h

Atom	U_{eq}	U_{11}	U_{22}	U_{33}	U_{23}	U_{13}	U_{12}
S	6.6(2)	6.7(2)	6.7(2)	6.5(3)	0	0	3.3(1)
Al	6.8(2)	4.7(3)	5.9(3)	9.5(3)	0.0(1)	0.1(3)	2.3(2)
O1	11.0(5)	13.3(7)	13.3(7)	6.2(9)	0	0	6.7(3)
O2	9.9(3)	11.7(5)	11.7(5)	9.9(6)	0.4(2)	−0.4(2)	8.4(5)
O3	8.6(3)	6.0(4)	6.0(4)	13.5(6)	−1.0(2)	1.0(2)	2.8(5)
K, Na, O4	14.0(4)	15.9(4)	15.9(4)	10.4(5)	0	0	8.0(2)
H	33.2(10)						
a (Å)	6.9741(3)	R_{int}	0.0348				
c (Å)	17.190(2)	Unique reflections	388				
V (Å³)	724.08	Unique $|F_o| > 4\sigma_F$	380				
Space group	$R\bar{3}m$	Refinement method	Least squares on F^2				
$F(000)$	624.0	Parameters varied	30				
Radiation	Mo Kα	R_1 for $|F_o| > 4\sigma_F$	0.0299				
Total reflections	4368	R_1 all data	0.0314				
Data range (2Θ)	3–69	wR_2 all data	0.0698				
D_x	2.84	Goodness of fit all data	1.264				
Crystal size	~200 µm	Max. min. peaks (e/Å³)	0.46, −0.43				

and trivalent cations are frequently partially vacant in the structure of the minerals of the alunite-jarosite group (Stoffregen et al. 2000). Our sample, however, has almost full occupancy of these sites (Table 1). The only elements detected in the electron microprobe (EMP) analyses were Al, Na, K, and S. Fe, Mn, Mg, and Ca are absent. The terminal portions of the alunite crystals show oscillatory zoning (Fig. 2); the central parts of the crystals are homogeneous, representing by the medium-gray phase in Fig. 2. Brillouin spectra were collected from the central parts of the alunite crystals. The average of the Na/(Na + K) ratio in all zones is 0.14 ± 0.04 (two standard deviations of the mean, $n = 10$). We do not report the EPM analyses because of their scatter due to damage and release of volatiles observable during the exposure of the sample to the electron beam. Widening of the electron beam did not stabilize the analytical results, and therefore we consider the EMP analyses only as a semiquantitative information.

The powder XRD pattern showed only peaks that conform to the $R\bar{3}m$ symmetry of alunite. The refined lattice parameters are $a = 6.9789(9)$ Å and $c = 17.248(3)$ Å, in good agreement with previously published values for alunite (Stoffregen et al. 2000). Inspection of the crystals in polarized light also indicated absence of microscopic inclusions of other minerals, which could have interfered with the measurement. An uncrushed, flat single crystal was placed in the sample holder of the powder diffractometer, and the XRD pattern showed only (00ℓ) reflections, with $\ell = 3n$, where n is a positive integer. Therefore, the dominant forms on the crystals are the basal (001) pinacoids, terminated by small rhombohedral faces. The orientation of the platelet cut parallel to the dominant crystal faces was known and fixed at (001) during the analysis of the data. The orientation of the second platelet was refined together with the elastic constants during the data analysis to (−0.86, −0.72, 1).

A representative Brillouin spectrum is shown in Fig. 3. The measured velocities of all three modes were almost constant in the (001) plane (Fig. 4). In the plane (−0.86, −0.72, 1), only two modes were observed, with marked anisotropy of the velocities.

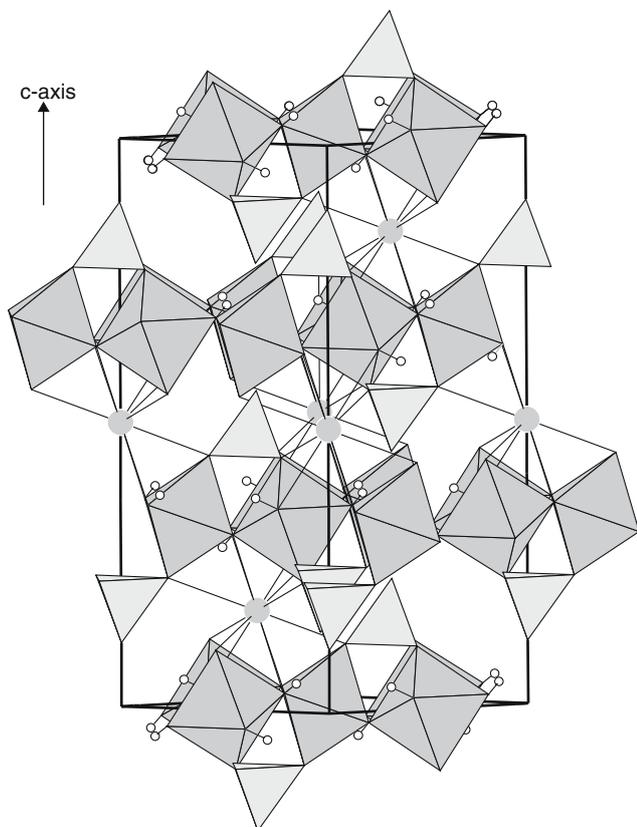Acoustic velocity can be determined from Brillouin frequency shift as

Fig. 1 A schematic drawing of the structure of alunite. *Light gray* are the sulfate tetrahedra, *medium gray* the aluminum octahedra. Potassium atoms shown as *large gray spheres*, hydrogen atoms as small white spheres. The unit cell is outlined in *thick solid lines*
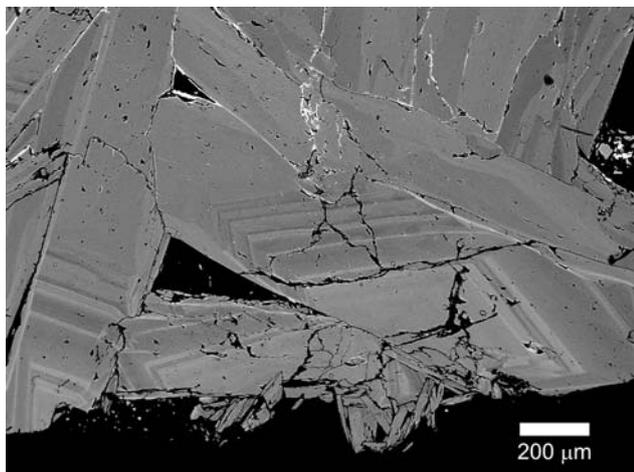

Fig. 3 A representative Brillouin spectrum of alunite. *LA* quasi-longitudinal acoustic mode, *TA* quasi-transverse acoustic modes, *R* unshifted Rayleigh line

$$v = (\lambda_0 \Delta v)/(2 \sin \alpha), \qquad (1)$$

where λ_0 is the incident laser wavelength, Δv is the Brillouin frequency shift, and α is the incidence angle. The acoustic velocity data and the density were inverted using a nonlinear least-squares fitting to analytical expressions of the solutions of the Christoffel's equation (Auld 1973; Every 1980):

$$(C_{iklm} l_k l_m - \rho v^2 \delta_{il})\, u_i = 0,$$

where C_{iklm} are the elastic constants in full notation (the elastic tensor is a four rank tensor), l_k and l_m are

Fig. 2 Back-scattered electron image of the alunite crystals. The spot analyses were acquired from the central portions of the crystals at different places in the sample. The white mineral along the fractures is an unidentified Fe-As phase. Scale represents 200 μm
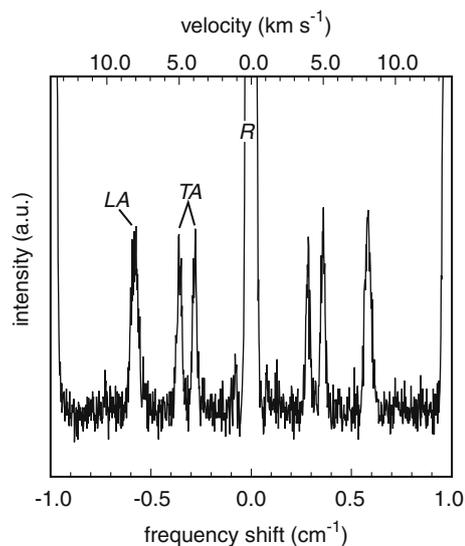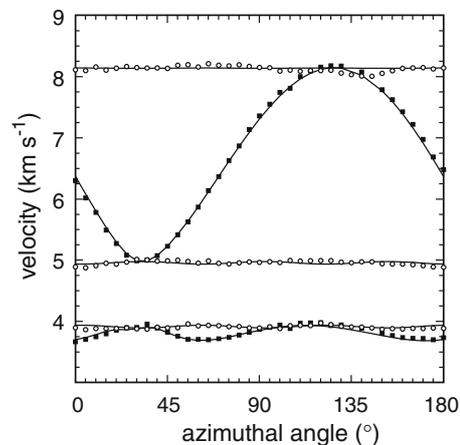

Fig. 4 Quasi-longitudinal and quasi-transverse acoustic velocities in the (001) (*white circles*) and (–0.86, –0.72, 1) (*black squares*) planes of an alunite crystal. The azimuthal angle is relative to an arbitrary starting direction. The solid curves are calculated using the best-fit elastic constants

the direction cosines of the elastic vibration, u_i is the local displacement vector, ρ is density, δ_{il} is the Kronecker delta. This set of equations admits three nontrivial solutions, which correspond to the velocities of the three polarizations of the acoustic vibration propagating along the selected direction. In the least-squares procedure the velocities were weighted by their $1\,\sigma$ experimental uncertainties.

Crystals with $R\bar{3}m$ symmetry have six nonzero elements in the elastic tensor, written in contracted notation (Nye 1985) as C_{11}, C_{33}, C_{12}, C_{13}, C_{44}, and C_{14}. The elastic constants C_{11}, C_{33}, C_{12}, and C_{44} were determined to a precision better than ±1% and the two less sensitive off-diagonal constants C_{13} and C_{14}, to a precision of ±4 and 10%, respectively. The accuracy and reproducibility of the elastic constants determined from the inversion of the measured velocity is better than 0.75% and it has been tested on reference materials (MgO, $MgAl_2O_4$) at ambient conditions (Speziale and Duffy 2002). The orientation of one of the platelets was refined to a precision of ±1°; the accuracy can be affected by trade-offs with the elastic constants (Speziale and Duffy 2002). The six constants determined by the fitting procedure are given in Table 2, together with elastic compliances, bulk and shear moduli, Poisson ratio, and elastic Debye temperature calculated from these constants. The root mean square deviation between the measured and calculated velocities is 0.04 km/s. The errors reported in Table 2 for C_{ij} are the estimated $1\,\sigma$ uncertainties from the least-squares fit.

Discussion

Alunite exhibits large anisotropy in the elastic constants. The value of C_{11} is much larger than that of C_{33}, the ratio C_{11}/C_{33} being 2.7. The ratio of basal versus meridian shear constants C_{66}/C_{44} is equal to 1.6. The elastic anisotropy of alunite is due to a denser atomic packing in the basal planes with respect to the c-axis. Large anisotropy in elastic constants is characteristic for layered compounds, for example for muscovite (McNeil and Grimsditch 1993), orpiment (McNeil and Grimsditch 1991), or graphite (Blakslee et al. 1970). Significant difference in the values of C_{11} and C_{33} are found in some other minerals with the same symmetry as alunite, e.g., tourmaline C_{11}/C_{33} ~1.7 (Ozkan 1979) and brucite C_{11}/C_{33} ~3.4 (Xia et al. 1998).

In terms of elastic properties, the trigonal structure of alunite exhibits a pseudo-hexagonal behavior at ambient conditions. In fact, the elastic anisotropy within the basal plane, controlled by the absolute value

of the constant C_{14}, is of the order of 0.1% for the longitudinal acoustic velocity and 0.9 and 1.1% for the two polarizations of the transverse acoustic velocity.

The Voigt and Reuss bounds to the aggregate bulk modulus of alunite are 70.6 and 54.5 GPa, those of the shear modulus are 52.4 and 46.3 GPa, respectively. The large difference (~30%) between the Voigt and Reuss bounds of the bulk modulus is a consequence of the high degree of elastic anisotropy. Alunite exhibits a large shear modulus in comparison with the bulk modulus, which is reflected in low Poisson's ratio value of 0.188 (Table 2). There are few elastic tensor measurements on minerals of related chemical composition. The hydrated sulfate gypsum ($CaSO_4 \cdot 2H_2O$) has a comparable bulk modulus of 45 ± 1 GPa, as inferred from static compression data (Stretton et al. 1997).

The layered nature of the structure of alunite strongly affects also the Debye temperature (Fig. 5). The Debye temperature calculated from the heat capacity (C_p) data changes markedly over the interval 0–300 K, and does not reach a plateau. Such trend is characteristic for strongly anisotropic structures (see Kieffer 1979). In addition, the elastic Debye temperature (Table 2, Fig. 5) deviates significantly from the C_p

Table 2 Elastic constants C_{ij} (GPa), compliances s_{ij} (10^{-12} Pa^{-1}), bulk and shear moduli K and G (GPa), Poisson's ratio v, and elastic Debye temperature Θ_{el} (K) for alunite ($\rho = 2.75$ g cm^{-3}) and jarosite

	Alunite	Jarosite
C_{11}	181.9 ± 0.3	189.0
C_{33}	66.8 ± 0.8	50.8
C_{44}	42.8 ± 0.2	36.0
C_{66}	66.9 ± 0.3	66.8
C_{12}	48.2 ± 0.5	55.5
C_{13}	27.1 ± 1.0	27.2
C_{14}	5.4 ± 0.5	6.8
s_{11}	6.18 ± 0.06	6.140
s_{33}	16.6 ± 0.3	22.35
s_{44}	23.6 ± 0.2	28.32
s_{12}	-1.38 ± 0.06	−1.497
s_{66}	15.11 ± 0.18	15.274
s_{13}	-1.95 ± 0.08	−2.486
s_{14}	-0.95 ± 0.09	−1.443
K_V	70.6 ± 0.5	72.1
K_R	54.5 ± 0.5	46.1
K_{VRH}	62.6 ± 0.7	59.1
G_V	52.4 ± 0.2	49.0
G_R	46.3 ± 0.2	39.5
G_{VRH}	49.4 ± 0.3	44.3
v	0.188 ± 0.004	0.20
Θ_{el}	654	571

Elastic constants for jarosite were calculated by GULP, using potentials from Becker and Gasharova (2001). The values of K, G, and Θ_{el} were calculated from expressions in Anderson (1963). $C_{66} = 0.5 \times (C_{11} - C_{12})$. $s_{66} = 2 \times (s_{11} - s_{12})$
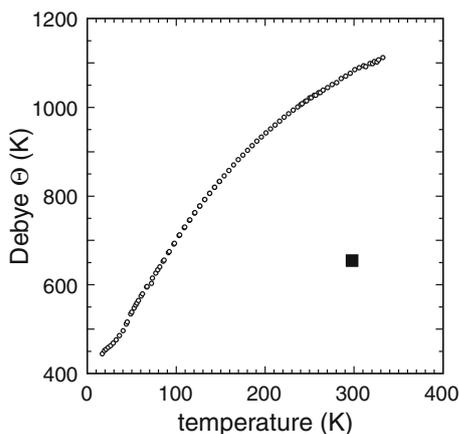
Fig. 5 Heat capacity Debye Θ (*small white circles*) and the elastic Debye Θ (*large black square*) for alunite. Heat capacity data for alunite taken from Hemingway and Robie (1994)

Debye temperature, because the simple Debye model of a vibrational continuum breaks down for the complicated structure of alunite.

We are not aware of any previously published elasticity measurements in alunite or an isostructural compound. The results of this study can be only compared with the calculated elastic constants of jarosite (Table 2). These constants were computed using the code GULP (Gale 1997) and the interatomic potentials derived by Becker and Gasharova (2001). Strictly speaking, it is difficult to compare the measured elastic constants of alunite and the calculated ones for jarosite. The calculated constants for jarosite are only a prediction whose uncertainty is unknown. On the other hand, the measured constants for alunite are likely to be more accurate and the precision of the measurement is known and reported in this paper. Nevertheless, we attempt to compare the two sets of data, perhaps only to point out where the main differences lie and to guide anyone who would want to derive interatomic potentials for alunite.

The C_{11}/C_{33} ratio of 3.7 for jarosite is considerably bigger than that for alunite $C_{11}/C_{33} = 2.7$. The VRH average shear modulus for alunite is about 10% greater than for jarosite. The shear modulus C_{66} in the octahedral layers is very similar for the two materials, but the resistance to shear normal to layering C_{44} is smaller for jarosite. The substitution of Fe for Al has only modest effects on the "in layer" elastic constants C_{11} and C_{66}. On the other hand, the differences in C_{44} and C_{11}/C_{33} are significant. It is surprising that the main effect of Fe-Al substitution is on the elastic constants normal to layering. The *c* parameters of alunite and jarosite are comparable, but the *a* parameter of jarosite (7.3 Å) is significantly larger than the parameter of alunite (7.0 Å). Therefore, one would expect to

observe the largest difference in the "in layer" elastic constants, in contrast with the comparison of the experimentally measured constants for alunite and calculated constants for jarosite. A high pressure XRD investigation could resolve the discrepancies and elucidate the mechanism of compression in these structures.

References

Anderson OL (1963) A simplified method for calculating the Debye temperature from elastic constants. J Phys Chem Solids 24:909–917

Auld B (1973) Acoustic fields and waves in solids, vol. 1. Wiley, New York

Becker U, Gasharova B (2001) AFM observations and simulations of jarosite growth at the molecular scale: probing the basis for the incorporation of foreign ions into jarosite as a storage mineral. Phys Chem Miner 28:545–556

Blakslee OL, Proctor DG, Seldin EJ, Spence GB, Weng T (1970) Elastic constants of compression-annealed pyrolytic graphite. J Appl Phys 41:3373–3382

Blaney DL, McCord TB (1995) Indications of sulfate minerals in the Martian soil from Earth-based spectroscopy. J Geophys Res-Planet 100(E7):14433–14441

Blowes DW, Jambor JL, Hanton-Fong CJ, Lortie L, Gould WD (1998) Geochemical, mineralogical and microbiological characterization of a sulphide-bearing carbonate-rich goldmine tailings impoundment, Joutel, Quebec. Appl Geochem 13:687–705

Cravotta CA III, Brady KBC, Rose AW, Douds JB (1999) Frequency distribution of the pH of coal-mine drainage in Pennsylvania. In: Morganwalp DW, Buxton H (eds) U.S. geological survey toxic substances hydrology program- proc technical meeting. US Geol Surv, Water-Res Invest Rep 99-4018A, pp 313–324

Every AG (1980) General closed-form expressions for acoustic waves in elastically anisotropic solid. Phys Rev B 22:1746–1760

Gale JD (1997) GULP: a computer program for the symmetry adapted simulation. J Chem Soc Faraday Trans 93:629–637

Hemingway BS, Robie RA (1994) Heat capacity and enthalpy of formation of synthetic alunite. US Geol Surv Open-file Rep 94-688, 8 pp

Hendricks SB (1937) The crystal structure of alunite and the jarosites. Am Mineral 22:773–784

Hudson-Edwards KA, Schell C, Macklin MG (1999) Mineralogy and geochemistry of alluvium contaminated by metal mining in the Rio Tinto area, southwest Spain. Appl Geochem 14:1015–1030

Ibers JA, Hamilton WC (eds) (1974) International tables for X-ray crystallography. IV revised and supplementary tables, vol. 4. The Kynoch Press, Birmingham, UK

Jambor JL, Nordstrom DK, Alpers CN (2000) Metal-sulfate salts from sulfide mineral oxidation. Rev Mineral Geochem 40:303–350

Jiang FM, Speziale S, Duffy TS (2004) Single-crystal elasticity of grossular- and almandine-rich garnets to 11 GPa by Brillouin scattering. J Geophys Res-Sol Ea 109:B10210

Kieffer SW (1979) Thermodynamics and lattice-vibrations of minerals. 1. Mineral heat-capacities and their relationships to simple lattice vibrational models. Rev Geophys 17:1–19

Klingelhofer G, Morris RV, Bernhardt B, Schroder C, Rodionov DS, de Souza PA, Yen A, Gellert R, Evlanov EN, Zubkov B, Foh J, Bonnes U, Kankeleit E, Gutlich P, Ming DW, Renz F, Wdowiak T, Squyres SW, Arvidson RE (2004) Jarosite and hematite at Meridiani Planum from Opportunity's Mössbauer spectrometer. Science 306:1740–1745

Larson AC, von Dreele RB (1994) GSAS. General structure analysis system. LANSCE, MS-H805, Los Alamos, NM

Lindsay SM, Anderson MW, Sandercock JR (1981) Construction and alignment of a high-performance multipass Vernier tandem Fabry-Perot interferometer. Rev Sci Instrum 52:1478–1486

McCord TB, Hansen GB, Hibbitts CA (2001) Hydrated salt minerals on Ganymede's surface: evidence of an ocean below. Science 292:1523–1525

McNeil LE, Grimsditch M (1991) Elastic-constants of As_2S_3. Phys Rev B 44:4174–4177

McNeil LE, Grimsditch M (1993) Elastic moduli of muscovite mica. J Phys Condens Matter 5:1681–1690

Nye JF (1985) Physical properties of crystals. Their representation by tensors and matrices. Oxford Science Publications, Oxford, p 329

Ozkan H (1979) Elastic constants of tourmaline. J Appl Phys 50:6006–6007

Schukow H, Breitinger DK, Zeiske T, Kubanek F, Mohr J, Schwab RG (1999) Localization of hydrogen and content of oxonium cations in alunite via neutron diffraction. Z Anorg Allg Chem 625:1047–1050

Speziale S, Duffy TS (2002) Single-crystal elastic constants of fluorite (CaF_2) to 9.3 GPa. Phys Chem Miner 29:465–472

Stoffregen RE, Alpers CN (1992) Observations on the unit cell parameters, water contents and δD of natural and synthetic alunites. Am Mineral 77:1092–1098

Stoffregen RE, Alpers CN, Jambor JL (2000) Alunite-jarosite crystallography, thermodynamics, and geochronology. Rev Mineral Geochem 40:454–480

Stretton IC, Schofield PF, Hull S, Knight KS (1997) The static compressibility of gypsum. Geophys Res Lett 24:1267–1270

Zolotov MY, Shock EL (2001) Composition and stability of salts on the surface of Europa and their oceanic origin. J Geophys Res-Planet 106(E12):32815–32827

Xia X, Weidner DJ, Zhao H (1998) Equation of state of brucite: single crystal Brillouin spectroscopy study and polycrystalline pressure-volume-temperature measurement. Am Mineral 83:68–74